THE JOURNAL OF PHYSICAL CHEMISTRY Letters

Letter

pubs.acs.org/JPCL

Single-Particle Spectroscopic Study on Fluorescence Enhancement by Plasmon Coupled Gold Nanorod Dimers Assembled on DNA Origami

Taishi Zhang,[†,‡] Nengyue Gao,[§] Shuang Li,[§] Matthew J. Lang,*[,‡,⊥] and Qing-Hua Xu*[,†,‡,§]

[†]NUS Graduate School for Integrative Sciences & Engineering, Singapore 117456

[‡]BioSyM IRG, Singapore−MIT Alliance for Research and Technology, Singapore 138602

[§]Department of Chemistry, National University of Singapore, Singapore 117543

[⊥]Department of Chemical and Biomolecular Engineering and Department of Molecular Physiology and Biophysics, Vanderbilt University, Nashville, Tennessee 37235, United States

Supporting Information

ABSTRACT: Metal-enhanced fluorescence has attracted much attention due to its scientific importance and lots of potential applications. Plasmon coupled metal nanoparticles have been demonstrated to further improve the enhancement effects. Conventional studies of metal-enhanced fluorescence on the bulk systems are complicated by the ensemble average effects over many critical factors with large variations. Here, fluorescence enhancement of ATTO-655 by a plasmon coupled gold nanorod dimer fixed on a DNA origami nanobreadboard was studied on the single-particle level. A series of gold nanorod dimers with linear orientation and different gap distances ranging from 6.1 to 26.0 nm were investigated to explore the plasmon coupling effect on fluorescence enhancement. The results show that the dimer with the smallest gap (6.1 nm) gives the highest enhancement (470-fold), and the enhancement gradually decreases as the gap distance increases and eventually approaches that from a monomer (120-fold). This trend is consistent with the numerical calculation results. This study indicates that plasmon coupling in gold nanorod dimers offers further increased excitation efficiency to achieve large fluorescence enhancement.

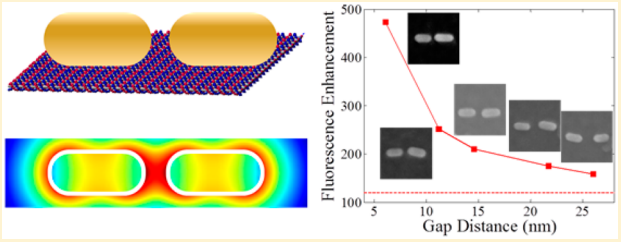

Rapid development in metal-enhanced optical properties has been achieved in the last few decades. When a chromophore comes to the proximity of metal nanoparticles (NPs), the optical responses of the chromophore will be modulated significantly, such as surface-enhanced Raman scattering (SERS) and metal-enhanced fluorescence (MEF).[1] The enhanced optical responses of the chromophore arise from their interactions with localized surface plasmon resonance (LSPR) of noble metal NPs.[2,3] SERS has been extensively studied for the last few decades.[4] MEF has emerged since the 1990s as an exciting new research area with a lot of potential applications. Metal−chromophore interactions can result in local electric field amplification, enhanced radiative decay rates of the chromophore, and nonradiative energy transfer from the chromophore to metal NPs. These three processes will modulate the excitation and emission efficiency of the chromophore and result in potentially enhanced fluorescence.[5] MEF was initially discovered on the film substrates[6,7] and later demonstrated in the colloid solutions.[8,9] The extent of fluorescence enhancement is strongly dependent on the particle size,[10,11] shape,[12,13] spectral overlap,[14,15] and separation distance[9,16] between the chromophores and metal NPs. Most previous studies were conducted in the bulk films or colloid solutions, in which there is a large variation in particle size and shape, metal−chromophore distance, as well as spectral overlap. The observed results in these studies are ensemble-averaged over many metal−chromphore pairs with large variations. Single-particle spectroscopy allows direct measurement of optical properties of individual metal NPs and thus effectively eliminates the ensemble average effects due to the above-mentioned variations to allow better understanding the metal−chromophore interactions. For example, fluorescence enhancement by gold nanorods (Au NRs) has been reported to be ∼10-fold in bulk ensemble measurements,[9,17] while a single-particle study showed that the maximum fluorescence enhancement can reach up to 1000-fold.[18]

When two metal NPs are brought into close proximity, coupling interactions between their LSPR modes can lead to formation of an electric field hotspot in the gap, which results in huge enhancement in optical responses such as SERS and fluorescence.[19] The enhancement factors of SERS and fluorescence by the plasmon coupled NPs have been demonstrated to be a few orders of magnitude higher than that by uncoupled NPs.[20,21] It is attractive to develop

Received: April 10, 2015
Accepted: May 13, 2015
Published: May 13, 2015

DOI: 10.1021/acs.jpclett.5b00747
J. Phys. Chem. Lett. 2015, 6, 2043−2049

reproducible plasmon coupled nanostructures for enhanced optical responses. Two strategies are generally used to fabricate such nanostructures: top-down and bottom-up. Top-down refers to nanolithography techniques using an electron beam[22,23] or focused ion beam.[24] These techniques provide consistent output with well-controlled shape and gap distance. However, the high equipment cost and complexity of operation prevent such methods from being widely available. In comparison, bottom-up strategy by a variety of wet chemistry methods offers a relatively inexpensive alternative.[25−28] DNA origami has recently been utilized to arrange metal NPs into ordered patterns because of its excellent spacing controllability and large-scale productivity.[29−31] A few efforts have been made to use DNA origami to form coupled metal nanosphere dimers to achieve SERS and MEF both in a bulk colloid system[32] and on the single-particle level.[33,34] So far, these studies were mainly focused on spherical NPs. Au NRs have been known to display larger fluorescence enhancement than Au nanospheres.[17,18] Furthermore, Au NRs display some unique advantages such as strong field enhancement,[35] weak plasmon damping,[36] and a tunable LSPR band ranging from 600 nm to the near-infrared. Au NRs are expected to be more effective in enhancing the fluorescence of red and near-IR dyes because their LSPR bands can be tuned to match the spectra of red/near-IR dyes to achieve optimal fluorescence enhancement. Au NR-based nanostructures with enhanced red/near-IR emission are particularly useful in bioimaging applications because excitation and emission in the red/near-IR region allow deeper penetration into biological tissues with less photodamage and autofluorescence from the tissues.[37]

Here, we report a single-particle study on the fluorescence enhancement of a bright red emitter, ATTO-655, by DNA origami nanobreadboard coupled Au NR dimers with a linear orientation and different gap distances. ATTO-655 was chosen because of its high brightness, excellent photostability, and good spectral overlap with Au NRs, making it suitable for single-molecule fluorescence studies. Single-molecule fluorescence studies on fluorescence enhancement of ATTO-655 in these Au NR dimers with five different gap distances (from 6.1 to 26.0 nm) were conducted to understand how fluorescence enhancement is affected by plasmon coupling. The enhancement capability was found to decrease as the gap distance increased. Finite difference time domain (FDTD) simulations have been further conducted to understand the plasmon coupling effect on the fluorescence enhancement. This study provides insight into understanding the fluorescence enhancement mechanism and designing plasmonic nanostructures for optimal enhancement effects.

The procedure of coupling two Au NRs into a tip-to-tip dimer is schematically shown in Figure 1a. First, two orthogonal sets of short DNA oligonucleotides (red and yellow) were coated onto Au NRs via thiol groups. Correspondingly, two sets of the DNA origami staples were modified with extended tails (green and purple) in order to bind complimentarily to the thiolated oligonucleotides that were coated onto Au NRs. When annealed together, the complementary DNA oligonucleotides specifically coupled the nanobreadboard and Au NRs through the hybridization interactions. UV−vis extinction spectra (Figure 1b) showed that the longitudinal LSPR band maxima of Au NRs red-shifted from 625 to 641 nm after the hybridization, confirming the plasmon coupling interactions between adjacent Au NRs in the formed dimer. The absorption band at 260 nm (blue arrow in

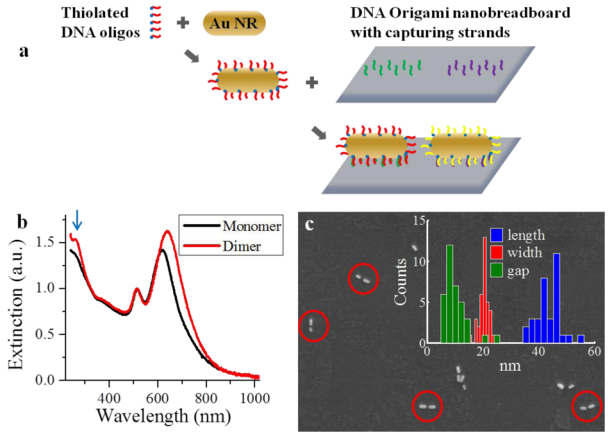

Figure 1. (a) Schematic design of Au NR dimers coupled by a nanobreadboard; (b) UV−vis extinction spectra of solutions containing Au NR monomers (black) and coupled Au NR dimers (red); (c) SEM image of coupled Au NR dimers (the inset is the size distribution).

Figure 1b) in the dimer is due to the characteristic absorption of DNA. The morphology of the dimer was characterized by scanning electron microscopy (SEM) images (Figures 1c and S5 (Supporting Information)). Statistics based on 37 dimers gave size distributions of 43.5 ± 4.6 nm for length, 20.4 ± 2.0 nm for width, and 11.1 ± 4.3 nm for gap (Figure 1c, inset). FDTD simulations show that the Au NR with the above-measured geometry gave a LSPR peak at 625 nm for the monomer and 650 nm for a dimer with a gap of 10 nm, which is in good overlap with the absorption and fluorescence spectra of ATTO-655 (λ_{abs} = 663 nm, λ_{em} = 682 nm, fluorescence quantum yield (QY) = 0.3) to achieve fluorescence enhancement (Figure S2b, Supporting Information).

Single-molecule fluorescence experiments were performed using the setup shown in Figure 2a. A 642 nm CW laser served as the excitation source. The laser beam was expanded five times by using a pair of lenses, and its polarization was adjusted by using a half-wave plate before focusing onto the sample

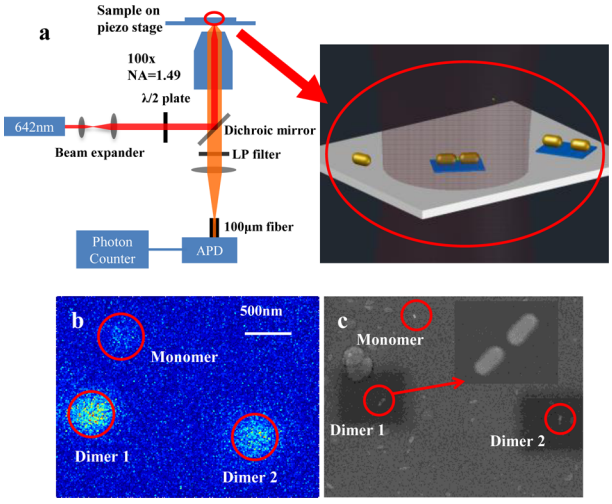

Figure 2. (a) Experimental setup for measuring the fluorescence intensity time trace of single ATTO-655 molecules flowing through a nanobreadboard coupled Au NR dimer. (b,c) Pattern matching between the photoluminescence scanning image (b) and SEM image (c); the inset of (c) is the high magnification SEM image of dimer 1.

DOI: 10.1021/acs.jpclett.5b00747
J. Phys. Chem. Lett. 2015, 6, 2043−2049

through an objective lens (Nikon, 100× , NA = 1.49). The fluorescence signals were detected by an APD after passing through a 100 μm optical fiber and a long-pass emission filter with a cutoff wavelength at 664 nm. Fluorescence counts were recorded by using a photon counter. Au NR dimers were drop-casted onto an indium tin oxide (ITO) coverslip for SEM and then UV-ozone-treated before being incorporated within a homemade flow cell (Figure S6, Supporting Information) filled with 50 nM ATTO-655. At this concentration, the average number of ATTO-655 within the laser focal volume ($\sim$0.5 × 10^{-15}L) was 7.5 molecules (see detail calculation in the Supporting Information). Individual ATTO-655 molecules approached the surface-immobilized Au NR dimer by diffusion. Considering that the field enhancement is confined to a few tens of nm, the enhancement volume was on the order of a zeptoliter (10^{-21} L). Therefore, only a very small fraction of molecules within the focal volume were expected to experience fluorescence enhancement. Such rare enhancement events correspond to a series of temporally separated bursts over the background signals in the fluorescence intensity time trace. By monitoring these fluorescence bursts, fluorescence enhancement is resolved at the single-molecule level. For a sufficiently long observation time, fluorophores within the focal volume will probe the hotspot where the burst signal is highest. To make it easier to detect a fluorescence burst when an ATTO-655 molecule enters the hotspot, ATTO-655 was functionalized with a streptavidin, which effectively generates a larger hydrodynamic radius[38] and increases the diffusion time across the gap. A 1 × PBS buffer solution was utilized to provide conditions appropriate for the biological components of the assay. The solution was purged with nitrogen to minimize photobleaching during the fluorescence measurements. A laser power of 8.0 μW (corresponding to a power density of 2.8 kW/cm^2) was used to minimize damage to the sample.

The Au NR dimers of interest were identified through a pattern-matching method by correlating the photoluminescence scanning image (Figure 2b) to the SEM image (Figure 2c). The Au NR dimers with desired gap distance and orientation were first identified by the SEM image. The same area was then imaged on the optical microscope shown in Figure 2a by monitoring the photoluminescence under laser excitation at 642 nm. By comparing the photoluminescence patterns with the SEM images, the location of the targeted Au NR dimer was identified for the subsequent fluorescence enhancement studies. In the following session, dimer 1 of Figure 2b was used as an example to illustrate how fluorescence enhancement measurements were performed. As shown in the inset of Figure 2c, dimer 1 had a tip-to-tip orientation with a gap distance of 14.6 nm. When immersed into the ATTO-655 solution, ATTO-655 molecules could diffuse through the gap region, and their fluorescence intensities got enhanced. The fluorescence intensity time trace was recorded for 10 min. The excitation polarization was adjusted to be parallel to the long axis of the Au NR dimer (red curves in Figure 3). The control experiments were also done to measure the fluorescence intensity time trace at a spot without any Au NR dimer for background fluorescence (black curves in Figure 3). Compared to the control spot, the fluorescence intensity traces of ATTO-655 in the presence of the Au NR dimer showed two distinctive features: a series of enhanced bursts and an increased baseline. The enhanced bursts were attributed to the enhanced fluorescence of ATTO-655 molecules, while the increased baseline was due to the continuously emitting photo-

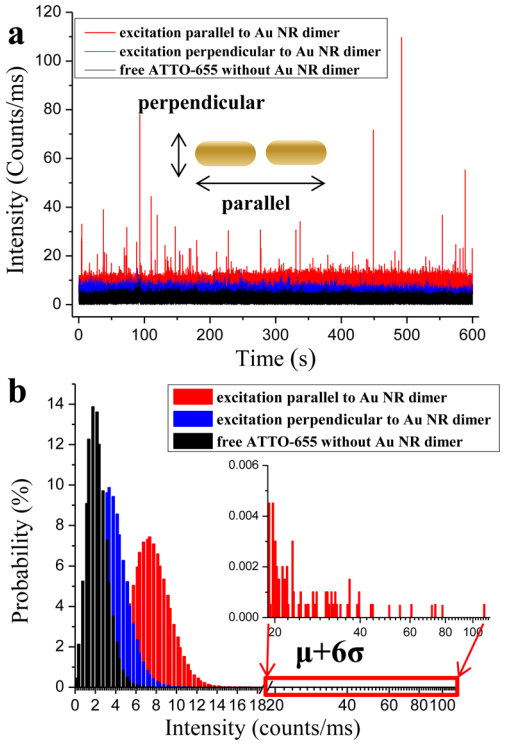

Figure 3. Fluorescence intensity time trace (a) and (b) counts histogram of dimer 1 under excitation along the parallel direction (red), perpendicular direction (blue), and control spot for free ATTO-655 without the Au NR dimer (black). The inset of (b) shows the zoomed data of bursts with probability beyond the (μ + 6σ) confident interval.

luminescence of the Au NR dimer itself. The difference could also be manifested by the intensity distribution in Figure 3b. Enhanced ATTO-655 fluorescence was revealed by the low probability yet high intensity counts beyond the 6σ confidence interval, as shown in Figure 3b, inset. The maximum intensity of these bursts gave 109.7 counts/ms. In the presence of the Au NR dimer, the fluorescence intensities shifted the major population from 1.8 to 7.3 counts/ms. A fluorescence enhancement factor was defined as the ratio of fluorescence intensity from an enhanced molecule over that from an unenhanced molecule. In order to calculate the enhancement factor, the intensity contributions by photoluminescence of the Au NR dimer and background fluorescence needed to be excluded. The net fluorescence intensity from the highest burst gave (109.7−7.3) = 102.4 counts/ms. Fluorescence from an unenhanced molecule was 1.8/7.5 = 0.24 counts/ms. Therefore, the enhancement factor was 102.4/0.24 $\approx$ 426. The fluorescence intensity was also measured with laser polarization perpendicular to the long axis of the Au NR dimer (the blue curves in Figure 3). In this case, the total fluorescence intensity showed only a slight increase due to the photoluminescence of the Au NR dimer itself, and no obvious enhanced burst was observed. This confirmed that the observed fluorescence enhancement originated from the interactions between the coupled longitudinal LSPR mode and the ATTO-655 molecules diffusing into the hotspot of the Au NR dimer.

Fluorescence enhancement (f_F) by metal NPs is a combined effect of excitation enhancement ($f_{|E|^2}$) and fluorescence QY enhancement (f_{QY}), $f_F = f_{|E|^2} \cdot f_{QY}$. Excitation enhancement originates from the enhanced local electric field and is

DOI: 10.1021/acs.jpclett.5b00747
J. Phys. Chem. Lett. 2015, 6, 2043−2049

proportional to $|E|^2$, which is expected to decrease monotonically with the increasing NP−fluorophore separation distance. QY enhancement involves two competing processes: radiative decay enhancement due to dipole−dipole interactions and an increased nonradiative decay rate due to resonant energy transfer from the fluorophore to the metal NP. If radiative decay enhancement dominates, the QY is enhanced ($f_{QY} > 1$); otherwise, if the increase in the nonradiative decay process dominates, the overall QY is quenched ($f_{QY} < 1$). As both radiative decay enhancement and resonant energy-transfer quenching are separation-distance-dependent, f_{QY} usually displays a quenching enhancement transition when the separation distance increases.[9,16,39] By using Au NR dimers with different gap distances, various metal NP−fluorophore distances could be sampled to study the gap distance dependence of fluorescence enhancement. Five Au NR dimers with gap distances of 6.1, 11.2, 14.6, 21.7, and 26.0 nm were identified by the SEM images (Figure 4a). These Au NR dimers

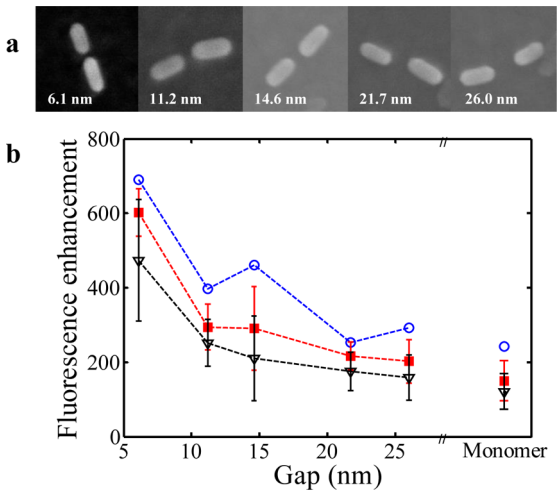

Figure 4. (a) SEM images of five Au NR dimers with different gaps. (b) Fluorescence enhancement based on the highest bursts, the averaged top 5−10 bursts for different Au NR dimers and a Au monomer.

had almost identical Au NR lengths and linearly aligned geometries. For direct comparison, experiments were also performed under identical conditions to investigate the fluorescence enhancement effect of a Au NR monomer. Figure 4b shows the fluorescence enhancement factors based on the highest bursts, the averaged top 5 and top 10 bursts, for Au NR dimers with different gap distances. The enhancement factors based on the highest bursts exhibit some degree of fluctuation due to the random Brownian motion that may cause imperfect Au NR−molecule alignment. In addition, there is still some rare possibility that multiple molecules enter the gap region together. Averaged results of the top 5 or top 10 bursts can effectively dilute these uncertainties and give a better representative trend for the gap-distance-dependent behavior (Figure 4b), although enhancement factors will be systematically underestimated. Using the averaged top 10 bursts to represent the enhancement factor, fluorescence enhancement of 473-, 252-, 210-, 175-, 158-, and 120-fold were obtained for Au NR dimers with gap distances of 6.1, 11.2, 14.6, 21.7, and 26.0 nm and a Au NR monomer, respectively. The coupled Au NR dimer with a gap distance of 6.1 nm gives a nearly 4-fold larger enhancement than that of the Au NR monomer (Figures 4b and S8 (Supporting Information)). As the gap distance increases, the enhancement factor gradually decreases and approaches that of a Au NR monomer.

Previously, researchers had demonstrated fluorescence enhancement exceeding 1000-fold for low QY (1.9−2.5%) dyes.[18,22] In general, the overall fluorescence enhancement is a product of enhancement in excitation efficiency and QY. The room for QY enhancement for low QY dyes is larger than that for high QY dyes because the QY cannot exceed 100%.[7,22] ATTO-655 has a QY of ∼0.3, and the QY enhancement is quite limited. Enhanced excitation efficiency is expected to play a dominant role in the overall fluorescence enhancement. To demonstrate different effects of enhanced QY and excitation efficiency and understand the gap-distance-dependent enhancement effects, numerical simulations have been performed by using the FDTD method.[40] Simulation results show that both electric field enhancement and QY enhancement depend on the location of the fluorophore within the gap as well as the gap distance. The spot with the largest excitation enhancement and the spot with the largest QY enhancement do not match (Figures S9 and S10, Supporting Information). For Au NR dimers with gap distances ranging from 4 to 35 nm, ATTO-655 has its QY maxima in the gap center. Its QY exhibits a mild dependence on the location when it is in the middle region and decreases sharply when it comes to the very close proximity of either Au NR. QY of ATTO-655 is actually slightly reduced as the increase in the nonradiative energy-transfer process plays a dominant role (Figure S10, Supporting Information). This is consistent with the previous studies on fluorophores with high intrinsic QY.[22] The excitation ($\propto|E|^2$) or electric field enhancement, however, displays a different trend. For a dimer with a large gap distance, the largest excitation enhancement spot is strongly biased toward the surface of either Au NR, while the excitation enhancement in the central region of the gap is much weaker. As the gap distance decreases, the excitation enhancement in the gap center grows stronger as a result of stronger plasmon coupling. The overall fluorescence enhancement is a balance between two effects. Consequently the optimum fluorescence enhancement is located somewhere between the gap center and the Au NR surface (Figures 5a and S10 (Supporting Information)). The optimum fluorescence enhancement location moves toward the gap center for the Au NR dimer with a smaller gap distance. Figure 5b summarizes the optimum fluorescence enhancement for Au NR dimers with different gap distances, as well as the corresponding contributions from the excitation efficiency and QY enhancement. As the gap distance decreases, the excitation efficiency increases significantly and reaches >1200-fold for a gap distance of 6.1 nm. In contrast, the QY is slightly reduced and displays a weaker dependence on the gap distance. Consequently, the overall fluorescence enhancement increases significantly as the gap distance decreases. The overall optimum fluorescence enhancement factors of 854-, 582-, 498-, 352-, and 317-fold were obtained for Au NR dimers with gap distances of 6.1, 11.2, 14.6, 21.7, and 26.0 nm, respectively, in comparison to 208-fold enhancement by a Au NR monomer (Figure S11, Supporting Information). The enhancement factors obtained from the simulation results for both Au NR dimers and monomers were about twice the experimental results. Two possible reasons are responsible for the underestimated experimental results. First, the experimental results were obtained by averaging the top 10 bursts, which is a conservative estimate of true enhancement factors. Second, nonideal experimental conditions, such as

DOI: 10.1021/acs.jpclett.5b00747
J. Phys. Chem. Lett. 2015, 6, 2043−2049

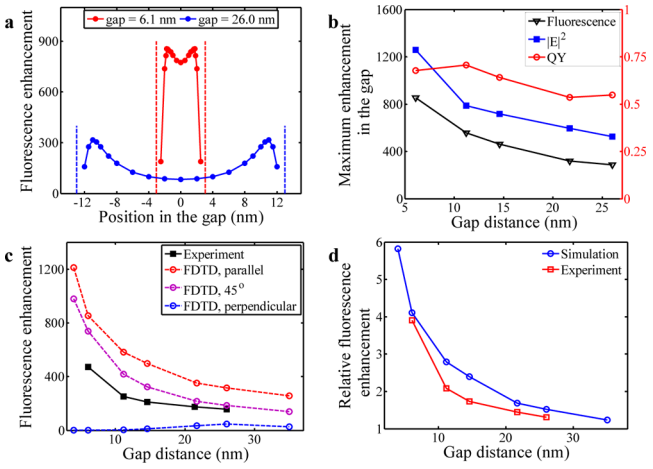

Figure 5. (a) Simulated fluorescence enhancement for Au NR dimers with gaps of 6.1 and 26.0 nm for the molecule dipole parallel to the long axis of the Au NR dimer. The vertical dashed lines indicate the boundary of gaps. (b) Simulated enhancement for QY (red), excitation (blue), and overall fluorescence (black) for different Au NR dimers with parallel molecular dipole orientation. (c) Comparison between the experimental results based on the averaged top 10 bursts and the simulation results for molecular dipole orientation parallel/perpendicular/45° to the long axis of the Au NR dimer. (d) Relative fluorescence enhancement of Au dimers normalized by that of the monomer for molecular dipole orientation parallel to the long axis of the Au NR dimer.

imperfect alignment of the fluorophore dipole with the orientation of the Au NR dimer, will result in lower enhancement factors. To understand the effect of molecular dipole orientation, simulations were performed on a dye molecule with the transition dipole moment parallel or perpendicular to the long axis of the Au NR dimer to represent two limiting cases and 45° orientation to represent a typical case (Figures 5c and S12 (Supporting Information)). The simulation results show that a dye molecule with the dipole parallel to the long axis of Au NR dimer experiences the largest enhancement, while a dye molecule with perpendicular dipole orientation experiences the lowest enhancement. A dye molecule with 45° orientation display fluorescence enhancement in-between the two limiting cases. Because these factors contribute similarly to both Au NR dimers and monomers, a relative enhancement factor was calculated by normalization of the enhancement factor of the dimers with respect to that of a monomer (Figure 5d). The experimental measurement and simulation results exhibit similar trends and excellent consistency; the relative enhancement factors gradually drop to 1 as the gap distance increases.

In conclusion, the fluorescence enhancement of a bright red emitter by plasmon coupled Au NR dimers fixed on a DNA origami nanobreadboard was studied on the single-particle level. A series of Au NR dimers with different gap distances ranging from 6.1 to 26.0 nm were investigated to explore the plasmon coupling effect on fluorescence enhancement. Au NR dimers with the narrowest gap gave the highest enhancement. A maximum enhancement factor of 470-fold was achieved at a gap distance of 6.1 nm, which is about 4 times larger than that of the Au NR monomer. As the gap distance increases, the enhancement factor of Au NR dimers decreases and approaches that of a Au NR monomer. This indicates that a metal NP dimer with stronger plasmon coupling is more efficient for fluorescence enhancement. These results were further supported by the FDTD numerical calculation results. The simulation results also indicate that enhanced excitation efficiency plays a dominant role in the overall fluorescence enhancement of ATTO-655.

EXPERIMENTAL METHODS

Au NR Preparation and LSPR Tuning. Au NRs were prepared by using a previously reported seed-mediated method.[41] The CTAB-stabilized seed solution was prepared by adding $HAuCl_4$ (0.01 M, 0.25 mL) and CTAB (0.1 M, 10 mL) solutions in a glass bottle. A freshly prepared ice-cold $NaBH_4$ (0.01 M, 0.6 mL) solution was then quickly added under vigorous stirring. The seed solution was mixed under vigorous stirring for 2 min and then kept at room temperature for at least 2 h before use. The growth solution was prepared by sequentially adding $HAuCl_4$ (0.01 M, 2.0 mL), $AgNO_3$ (0.01 M, 0.32 mL), HCl (1.0 M, 0.8 mL), and L-ascorbic acid (0.1 M, 0.32 mL) solutions into a CTAB (0.1 M, 40 mL) solution and mixed by swirling. Seed solution (100 μL) was then added into the reaction solution and gently mixed by inversion for 2 min. The resultant mixture was left undisturbed overnight. The UV−vis spectrum gave a LSPR peak at around 790 nm. Then, the LSPR of these Au NRs was tuned by H_2O_2 etching on the longitudinal direction.[41] Au NRs were mixed with 30% H_2O_2 at a volume ratio of 200:1 and kept at room temperature. The UV−vis extinction spectra were measured every 3 min until the LSPR peak approached the target wavelength of 625 nm. The reaction was stopped by centrifuging and resuspending the Au NRs in 0.01% SDS. The extinction cross section of such a Au NR was estimated to be 4.3×10^9 L·mol^{-1}·cm^{-1} (see details in the Supporting Information).

Self-Assembled DNA Origami Nanobreadboard. The rectangular nanobreadboard was prepared using Rothemund's method.[42] One single strand of M13mp18 DNA and 226 different strands of short "staples" (sequence shown in the Supporting Information) were mixed at a molar ratio of 1:5 and slowly annealed from 95 °C to room temperature at 1 °C/min in 1 × TAE-Mg^{2+} buffer. Atomic force microscopy (AFM) images showed that 63.5% of the structures displayed a rectangular morphology (Figure S3, Supporting Information).

Au NRs Coating with Thiolated DNA Oligonucleotide. Au NRs were split into two equal amounts and mixed with two sets of thiolated DNA oligonucleotides with sequences given in the appendix of the Supporting Information. The thiolated DNA oligonucleotide was reduced by excessive TCEP for 3 h before mixing with Au NRs at a molar ratio of 3000:1. After rotating the mixed solution at room temperature, 10 × TBE buffer was added to bring the final solution to 1 × TBE. The Au NR solution would retain its color if well coated; otherwise, they would aggregate under such buffer conditions. The mixed solution remained at room temperature for another 6 h before 5 M NaCl was added in 10 steps spanning 20 h to bring the final NaCl concentration to 0.5 M. The final mixture was rotated for another night before it was washed by centrifugation three times to remove excessive thiolated DNA oligonucleotide. The washed Au NRs were finally resuspended in 0.5 × TAE Mg^{2+} buffer and had the concentration measured again.

Hybridization between the Au NR and DNA Origami Nanobreadboard. The DNA origami was mixed with two sets of thiolated DNA oligonucleotide coated Au NRs at a molar ratio of 1:1:1 in 0.5 × TAE Mg^{2+} with 0.3 M NaCl. The mixture was heated repeatedly between 65 to 25 °C for 20 h. The final

DOI: 10.1021/acs.jpclett.5b00747
J. Phys. Chem. Lett. 2015, 6, 2043−2049

product was prepared for UV−vis spectrometry, electrophoresis, and SEM.

FDTD Simulation. FDTD simulations were performed by using the commercial software Lumerical FDTD Solutions. The simulation region was a 2 μm cube surrounded by a PML (perfectly matched layer) boundary condition. The Au NRs were placed in the center of the simulation region and were represented by hemisphere-capped cylinders with a geometry matched to the SEM image. The dielectric constant of gold was taken from Johnson and Christy's measurement[43] with polynomial fitting. A slab of an ITO-coated coverslip (refractive index = 1.9) was placed 3 nm beneath the structure. the refractive index of the rest of the simulation region was 1.33 for water. Excitation (|E|) enhancement and QY enhancement were simulated independently. For |E| simulation, light from a TFSF (total-field scattered-field) source with a spectrum ranging from 400 to 900 nm and polarization parallel to Au NR dimer coupling direction was injected from below the nanostructure. The spatial resolution was 0.3 nm near the gap and 0.5 nm elsewhere around the nanostructure. Mirror symmetry was used to reduce the simulation time and memory consumption. Two sets of power monitors forming a closed surface containing the structure were placed inside or outside of the light source region to measure absorption and scattering, respectively. Another three power monitors were placed at cross section planes of the x, y, z axes to record |E|. For QY simulations, the fluorophore was modeled as a dipole source. It was placed in the gap with dipole orientation parallel/perpendicular/45° to Au NR dimer coupling direction and emitting frequency that matched the fluorescence emission peak. Two sets of power monitors enclosed the a dipole-dimer system and dipole source, respectively, to calculate radiative decay rate enhancement f_R and nonradiative decay rate enhancement f_{NR}. Then, QY enhancement could be calculated by

$$f_{QY} = \frac{QY_m}{QY_0} = \frac{f_R}{(f_R + f_{NR})\cdot QY_0 + (1 - QY_0)}$$

■ ASSOCIATED CONTENT

Supporting Information

Design schematic of fixing Au NR dimers on a nanobreadboard; staple sequences of DNA origami; aspect ratio dependence of Au NR LSPR and spectral overlap of LSPR with fluorescence of ATTO-655 and laser excitation; estimation of the Au NR extinction coefficient; AFM image of a nanobreadboard; gel electrophoresis of a nanobreadboard with a Au NR dimer; more SEM images of the Au NR dimer fixed on a nanobreadboard; homemade flow cell; calculation of the laser excitation volume; comparison between the fluorescence time trace by the Au NR dimer and monomer; FDTD simulated |E| field distribution around the Au NR dimer and monomer; simulated enhancement factor for the QY, excitation, and fluorescence of Au NR dimers and monomer; and comparison of the simulation results for ATTO-655 molecules with a transition dipole moment parallel/perpendicular/45° to the long axis of the Au NR dimer. The Supporting Information is available free of charge on the ACS Publications website at DOI: 10.1021/acs.jpclett.5b00747.

■ AUTHOR INFORMATION

Corresponding Authors

*E-mail: matt.lang@vanderbilt.edu (M.J.L.).
*E-mail: chmxqh@nus.edu.sg (Q.H.X.).

Notes

The authors declare no competing financial interest.

■ ACKNOWLEDGMENTS

This work is supported by the National Research Foundation, Prime Minister's Office, Singapore under its Competitive Research Programme (CRP Award No. NRF-CRP10-2012-04) and Singapore−MIT Alliance of Research and Technology (SMART) Programme and the NUS Tier 1 Grant (R-143-000-607-112).

■ REFERENCES

(1) Geddes, C. D.; Lakowicz, J. R. Metal-Enhanced Fluorescence. *J. Fluoresc.* **2002**, *12*, 121−129.
(2) Willets, K. A.; Van Duyne, R. P. Localized Surface Plasmon Resonance Spectroscopy and Sensing. *Annu. Rev. Phys. Chem.* **2007**, *58*, 267−297.
(3) Hutter, E.; Fendler, J. H. Exploitation of Localized Surface Plasmon Resonance. *Adv. Mater.* **2004**, *16*, 1685−1706.
(4) Stiles, P. L.; Dieringer, J. A.; Shah, N. C.; Van Duyne, R. P. Surface-Enhanced Raman Spectroscopy. *Annu. Rev. Anal. Chem.* **2008**, *1*, 601−626.
(5) Anger, P.; Bharadwaj, P.; Novotny, L. Enhancement and Quenching of Single-Molecule Fluorescence. *Phys. Rev. Lett.* **2006**, *96*, 113002−113002.
(6) Lakowicz, J. R.; Shen, B.; Gryczynski, Z.; D'Auria, S.; Gryczynski, I. Intrinsic Fluorescence from DNA Can Be Enhanced by Metallic Particles. *Biochem. Biophys. Res. Commun.* **2001**, *286*, 875−879.
(7) Lakowicz, J. R.; Shen, Y.; D'Auria, S.; Malicka, J.; Fang, J.; Gryczynski, Z.; Gryczynski, I. Radiative Decay Engineering: 2. Effects of Silver Island Films on Fluorescence Intensity, Lifetimes, and Resonance Energy Transfer. *Anal. Biochem.* **2002**, *301*, 261−277.
(8) Tam, F.; Goodrich, G. P.; Johnson, B. R.; Halas, N. J. Plasmonic Enhancement of Molecular Fluorescence. *Nano Lett.* **2007**, *7*, 496−501.
(9) Abadeer, N. S.; Brennan, M. R.; Wilson, W. L.; Murphy, C. J. Distance and Plasmon Wavelength Dependent Fluorescence of Molecules Bound to Silica-Coated Gold Nanorods. *ACS Nano* **2014**, *8*, 8392−8406.
(10) Nakamura, T.; Hayashi, S. *Jpn. J. Appl. Phys.* **2005**, *44*, 6833.
(11) Stranik, O.; Nooney, R.; McDonagh, C.; MacCraith, B. D. Optimization of Nanoparticle Size for Plasmonic Enhancement of Fluorescence. *Plasmonics* **2007**, *2*, 15−22.
(12) Bardhan, R.; Grady, N. K.; Cole, J. R.; Joshi, A.; Halas, N. J. Fluorescence Enhancement by Au Nanostructures: Nanoshells and Nanorods. *ACS Nano* **2009**, *3*, 744−752.
(13) Liu, S.-Y.; Huang, L.; Li, J.-F.; Wang, C.; Li, Q.; Xu, H.-X.; Guo, H.-L.; Meng, Z.-M.; Shi, Z.; Li, Z.-Y. Simultaneous Excitation and Emission Enhancement of Fluorescence Assisted by Double Plasmon Modes of Gold Nanorods. *J. Phys. Chem. C* **2013**, *117*, 10636−10642.
(14) Chen, Y.; Munechika, K.; Ginger, D. S. Dependence of Fluorescence Intensity on the Spectral Overlap between Fluorophores and Plasmon Resonant Single Silver Nanoparticles. *Nano Lett.* **2007**, *7*, 690−696.
(15) Khatua, S.; Paulo, P. M.; Yuan, H.; Gupta, A.; Zijlstra, P.; Orrit, M. Resonant Plasmonic Enhancement of Single-Molecule Fluorescence by Individual Gold Nanorods. *ACS Nano* **2014**, *8*, 4440−4449.
(16) Cheng, D.; Xu, Q.-H. Separation Distance Dependent Fluorescence Enhancement of Fluorescein Isothiocyanate by Silver Nanoparticles. *Chem. Commun.* **2007**, 248−250.
(17) Zhao, T.; Yu, K.; Li, L.; Zhang, T.; Guan, Z.; Gao, N.; Yuan, P.; Li, S.; Yao, S. Q.; Xu, Q.-H. Gold Nanorod Enhanced Two-Photon Excitation Fluorescence of Photosensitizers for Two-Photon Imaging

DOI: 10.1021/acs.jpclett.5b00747
J. Phys. Chem. Lett. 2015, 6, 2043−2049

and Photodynamic Therapy. *ACS Appl. Mater. Interfaces* **2014**, *6*, 2700−2708.
(18) Yuan, H.; Khatua, S.; Zijlstra, P.; Yorulmaz, M.; Orrit, M. Thousand-Fold Enhancement of Single-Molecule Fluorescence near a Single Gold Nanorod. *Angew. Chem., Int. Ed.* **2013**, *52*, 1217−1221.
(19) Halas, N. J.; Lal, S.; Chang, W.-S.; Link, S.; Nordlander, P. Plasmons in Strongly Coupled Metallic Nanostructures. *Chem. Rev.* **2011**, *111*, 3913−3961.
(20) Zhang, Y.; Walkenfort, B.; Yoon, J. H.; Schlücker, S.; Xie, W. Gold and Silver Nanoparticle Monomers Are Non-SERS-Active: A Negative Experimental Study with Silica-Encapsulated Raman-Reporter-Coated Metal Colloids. *Phys. Chem. Chem. Phys.* **2015**, DOI: 10.1039/C4CP05073H.
(21) Gill, R.; Tian, L.; Somerville, W. R.; Le Ru, E. C.; van Amerongen, H.; Subramaniam, V. Silver Nanoparticle Aggregates as Highly Efficient Plasmonic Antennas for Fluorescence Enhancement. *J. Phys. Chem. C* **2012**, *116*, 16687−16693.
(22) Kinkhabwala, A.; Yu, Z.; Fan, S.; Avlasevich, Y.; Müllen, K.; Moerner, W. Large Single-Molecule Fluorescence Enhancements Produced by a Bowtie Nanoantenna. *Nat. Photonics* **2009**, *3*, 654−657.
(23) Zoriniants, G.; Barnes, W. L. Fluorescence Enhancement through Modified Dye Molecule Absorption Associated with the Localized Surface Plasmon Resonances of Metallic Dimers. *New J. Phys.* **2008**, *10*, 105002−105013.
(24) Punj, D.; Mivelle, M.; Moparthi, S. B.; van Zanten, T. S.; Rigneault, H.; van Hulst, N. F.; García-Parajó, M. F.; Wenger, J. A Plasmonic 'Antenna-in-Box' Platform for Enhanced Single-Molecule Analysis at Micromolar Concentrations. *Nat. Nanotechnol.* **2013**, *8*, 512−516.
(25) Zhang, J.; Fu, Y.; Chowdhury, M. H.; Lakowicz, J. R. Metal-Enhanced Single-Molecule Fluorescence on Silver Particle Monomer and Dimer: Coupling Effect between Metal Particles. *Nano Lett.* **2007**, *7*, 2101−2107.
(26) Xu, L.; Kuang, H.; Xu, C.; Ma, W.; Wang, L.; Kotov, N. A. Regiospecific Plasmonic Assemblies for in Situ Raman Spectroscopy in Live Cells. *J. Am. Chem. Soc.* **2012**, *134*, 1699−1709.
(27) Barrow, S. J.; Funston, A. M.; Wei, X.; Mulvaney, P. DNA-Directed Self-Assembly and Optical Properties of Discrete 1D, 2D and 3D Plasmonic Structures. *Nano Today* **2013**, *8*, 138−167.
(28) Pramod, P.; Thomas, K. G. Plasmon Coupling in Dimers of Au Nanorods. *Adv. Mater.* **2008**, *20*, 4300−4305.
(29) Ding, B.; Deng, Z.; Yan, H.; Cabrini, S.; Zuckermann, R. N.; Bokor, J. Gold Nanoparticle Self-Similar Chain Structure Organized by DNA Origami. *J. Am. Chem. Soc.* **2010**, *132*, 3248−3249.
(30) Pal, S.; Deng, Z.; Wang, H.; Zou, S.; Liu, Y.; Yan, H. DNA Directed Self-Assembly of Anisotropic Plasmonic Nanostructures. *J. Am. Chem. Soc.* **2011**, *133*, 17606−17609.
(31) Lan, X.; Chen, Z.; Dai, G.; Lu, X.; Ni, W.; Wang, Q. Bifacial DNA Origami-Directed Discrete, Three-Dimensional, Anisotropic Plasmonic Nanoarchitectures with Tailored Optical Chirality. *J. Am. Chem. Soc.* **2013**, *135*, 11441−11444.
(32) Pal, S.; Dutta, P.; Wang, H.; Deng, Z.; Zou, S.; Yan, H.; Liu, Y. Quantum Efficiency Modification of Organic Fluorophores Using Gold Nanoparticles on DNA Origami Scaffolds. *J. Phys. Chem. C* **2013**, *117*, 12735−12744.
(33) Thacker, V. V.; Herrmann, L. O.; Sigle, D. O.; Zhang, T.; Liedl, T.; Baumberg, J. J.; Keyser, U. F. DNA Origami Based Assembly of Gold Nanoparticle Dimers for Surface-Enhanced Raman Scattering. *Nat. Commun.* **2014**, DOI: 10.1038/ncomms4448.
(34) Acuna, G.; Möller, F.; Holzmeister, P.; Beater, S.; Lalkens, B.; Tinnefeld, P. Fluorescence Enhancement at Docking Sites of DNA-Directed Self-Assembled Nanoantennas. *Science* **2012**, *338*, 506−510.
(35) Mohamed, M. B.; Volkov, V.; Link, S.; El-Sayed, M. A. The 'Lightning' Gold Nanorods: Fluorescence Enhancement of over a Million Compared to the Gold Metal. *Chem. Phys. Lett.* **2000**, *317*, 517−523.
(36) Sonnichsen, C.; Franzl, T.; Wilk, T.; von Plessen, G.; Feldmann, J.; Wilson, O.; Mulvaney, P. Drastic Reduction of Plasmon Damping in Gold Nanorods. *Phys. Rev. Lett.* **2002**, *88*, 077402−077402.
(37) Le Moal, E.; Fort, E.; Lévêque-Fort, S.; Cordelières, F. P.; Fontaine-Aupart, M. P.; Ricolleau, C. Enhanced Fluorescence Cell Imaging with Metal-Coated Slides. *Biophys. J.* **2007**, *92*, 2150−2161.
(38) Ebersole, R. C.; Miller, J. A.; Moran, J. R.; Ward, M. D. Spontaneously Formed Functionally Active Avidin Monolayers on Metal Surfaces: A Strategy for Immobilizing Biological Reagents and Design of Piezoelectric Biosensors. *J. Am. Chem. Soc.* **1990**, *112*, 3239−3241.
(39) Liu, Z.; Ricks, A. M.; Wang, H.; Song, N.; Fan, F.; Zou, S.; Lian, T. High-Resolution Imaging of Electric Field Enhancement and Energy-Transfer Quenching by a Single Silver Nanowire Using QD-Modified AFM Tips. *J. Phys. Chem. Lett.* **2013**, *4*, 2284−2291.
(40) Chowdhury, M. H.; Pond, J.; Gray, S. K.; Lakowicz, J. R. Systematic Computational Study of the Effect of Silver Nanoparticle Dimers on the Coupled Emission from Nearby Fluorophores. *J. Phys. Chem. C* **2008**, *112*, 11236−11249.
(41) Ni, W.; Kou, X.; Yang, Z.; Wang, J. Tailoring Longitudinal Surface Plasmon Wavelengths, Scattering and Absorption Cross Sections of Gold Nanorods. *ACS Nano* **2008**, *2*, 677−686.
(42) Rothemund, P. W. Folding DNA to Create Nanoscale Shapes and Patterns. *Nature* **2006**, *440*, 297−302.
(43) Johnson, P. B.; Christy, R.-W. Optical Constants of the Noble Metals. *Phys. Rev. B* **1972**, *6*, 4370−4379.

DOI: 10.1021/acs.jpclett.5b00747
J. Phys. Chem. Lett. 2015, 6, 2043−2049